arXiv:0908.0511v1 [astro-ph.HE] 4 Aug 2009

Radio Imaging of the Very-High-Energy γ-Ray Emission Region in the Central Engine of a Radio Galaxy

The VERITAS Collaboration, the VLBA 43 GHz M 87 Monitoring Team, the H.E.S.S. Collaboration, and the MAGIC Collaboration*

The full author list with affiliations can be found at the end of this paper

Abstract

The accretion of matter onto a massive black hole is believed to feed the relativistic plasma jets found in many active galactic nuclei (AGN). Although some AGN accelerate particles to energies exceeding 10^{12} electron Volts (eV) and are bright sources of very-high-energy (VHE) γ-ray emission, it is not yet known where the VHE emission originates. Here we report on radio and VHE observations of the radio galaxy M 87, revealing a period of extremely strong VHE γ-ray flares accompanied by a strong increase of the radio flux from its nucleus. These results imply that charged particles are accelerated to very high energies in the immediate vicinity of the black hole.

Active galactic nuclei (AGN) are extragalactic objects thought to be powered by massive black holes in their centres. They can show strong emission from the core, which is often dominated by broadband continuum radiation ranging from radio to X-rays and by substantial flux variability on different time scales. More than 20 AGN have been established as VHE γ-ray emitters with measured energies above 0.1 tera electron Volts (TeV); the jets of most of these sources are believed to be aligned with the line-of-sight to within a few degrees. The size of the VHE γ-ray emission region can generally be constrained by the time scale of the observed flux variability [1, 2] but its location remains unknown.

We studied the inner structure of the jet of the giant radio galaxy M 87, a known VHE γ-ray emitting AGN [3, 2, 4, 5] with a $(6.0 \pm 0.5) \times 10^9\,\mathrm{M}_\odot$ black hole [6], scaled by distance, located $16.7\,\mathrm{Mpc}$ (54 million light years) away in the Virgo cluster of galaxies. The angle between its plasma jet and the line-of-sight is estimated to lie between $15 - 25\,\mathrm{deg}$ (see supporting online text). The substructures of the jet, which are expected to scale with the Schwarzschild radius

*To whom correspondence should be addressed; E-mail: beilicke@physics.wustl.edu, or krawcz@wuphys.wustl.edu (VERITAS), cwalker@aoc.nrao.edu, or phardee@bama.ua.edu (VLBA), martin.raue@mpi-hd.mpg.de (H.E.S.S.), mazin@ifae.es, or robert.wagner@mpp.mpg.de (MAGIC).

$R_{\rm s}$ of the black hole[1], are resolved in the X-ray, optical and radio wavebands [7] (Fig. 1). High-frequency radio very long baseline interferometry (VLBI) observations with sub-milliarcsecond (mas) resolution are starting to probe the collimation region of the jet [8]. With its proximity, bright and well-resolved jet, and very massive black hole, M 87 provides a unique laboratory in which to study relativistic jet physics in connection with the mechanisms of VHE γ-ray emission in AGN.

VLBI observations of the M 87 inner jet show a well resolved, edge-brightened structure extending to within $0.5\,{\rm mas}$ ($0.04\,{\rm pc}$ or $70\,R_{\rm s}$) of the core. Closer to the core, the jet has a wide opening angle suggesting that this is the collimation region [8]. Generally, the core can be offset from the actual location of the black hole by an unknown amount [9], in which case it could mark the location of a shock structure or the region where the jet becomes optically thin. However, in the case of M 87 a weak structure is seen on the opposite side of the core from the main jet, which may be the counter-jet, based on its morphology and length [10, 11]. Together with the observed pattern in opening angles, this suggests that the black hole of M 87 is located within the central resolution element of the VLBI images, at most a few tens of $R_{\rm s}$ from the radio core (see supporting online text). Along the jet, previous monitoring observations show both near-stationary components [11] (pc-scale) and features that move at apparent superluminal speeds [12, 13] (100 pc-scale). The presence of superluminal motions and the strong asymmetry of the jet brightness indicate that the jet flow is relativistic. The near-stationary components could be related to shocks or instabilities, that can be either stationary, for example if they are the result of interaction with the external medium, or slowly moving if they are the result of instabilities in the flow.

A first indication of VHE γ-ray emission from M 87 was reported by the High Energy Gamma-Ray Astronomy (HEGRA) collaboration in 1998/99 [3]. The emission was confirmed by the High Energy Stereoscopic System (H.E.S.S.) in 2003-2006 [2], with γ-ray flux variability on time scales of days. M 87 was detected again with the Very Energetic Radiation Imaging Telescope Array System (VERITAS) in 2007 [4] and, recently, the short-term variability was confirmed with the Major Atmospheric Gamma-Ray Imaging Cherenkov (MAGIC) telescope during a strong VHE γ-ray outburst [5] in February 2008. Causality arguments imply that the emission region should have a spatial extent of less than $\approx 5\delta R_{\rm s}$, where δ is the relativistic Doppler factor. This rules out explanations for the VHE γ-ray emission on the basis of (i) dark matter annihilation [14], (ii) cosmic-ray interactions with the matter in M 87 [15], or (iii) the knots in the plasma jet (Fig. 1C). Leptonic [16, 17] and hadronic [18] VHE γ-ray jet emission models have been proposed. However, the location of the emission region is still unknown. The nucleus [19, 20], the inner jet [21] or larger structures in the jet, such as the knot HST-1 (Fig. 1C), have been discussed as possible sites [13]. Because the angular resolution of VHE experiments is of the order of $0.1\,{\rm deg}$, the key to identifying the location of the VHE γ-ray emission lies in connecting it to measurements at other wavebands with considerably higher spatial resolutions. An angular resolution more than six orders of magnitude better (less than

[1]The Schwarzschild radius of a black hole with the mass m is defined as $R_{\rm s} = 2Gm/c^2$, G is the gravitational constant, and c is the speed of light. The Schwarzschild radius defines the event horizon of the black hole.

6×10^{-8} degrees, corresponding to approximately $30\,R_{\rm s}$ in case of M 87) can be achieved with radio observations (Fig. 1).

We used the H.E.S.S. [22], MAGIC [23] and VERITAS [24] instruments to observe M 87 during 50 nights between January and May 2008, accumulating over $95\,{\rm h}$ of data (corrected for the detector dead times) in the energy range between $0.1\,{\rm TeV}$ and several 10's of TeV. Simultaneously, we monitored M 87 with the Very Long Baseline Array [25] (VLBA) at $43\,{\rm GHz}$ with a resolution of $0.21 \times 0.43\,{\rm mas}$ [26], corresponding to about $30 \times 60\,R_{\rm s}$, see [27]. During the first half of 2008, three X-ray pointings were performed with the Chandra satellite [28]. Our light curves are shown in Fig. 2.

We detected multiple flares at VHE in February 2008 with denser sampling, following a trigger sent by MAGIC [$\sim$23 h of the data published in [5]]. The short-term VHE variability, first observed in 2005 [2], is clearly confirmed and the flux reached the highest level observed so far from M 87, amounting to more than 10% of that of the Crab Nebula. At X-ray frequencies the innermost knot in the jet (HST-1) is found in a low state, whereas in mid February 2008 the nucleus was found in its highest X-ray flux state since 2000 [28]. This is in contrast to the 2005 VHE γ-ray flares [2], which happened after an increase of the X-ray flux of HST-1 over several years [29], allowing speculation that HST-1 might be the source of the VHE γ-ray emission [13]; no $43\,{\rm GHz}$ radio observations were obtained at that time. Given its low X-ray flux in 2008, HST-1 is an unlikely site of the 2008 VHE flaring activity.

Over at least the following two months, until the VLBA monitoring project ended, the $43\,{\rm GHz}$ radio flux density from the region within $1.2\,{\rm mas}$ of the core rose by 30% as compared with its level at the time of the start of the VHE flare and by 57% as compared with the average level in 2007 (Fig. 2). The resolution of the $43\,{\rm GHz}$ images corresponds to $30 \times 60\,R_{\rm s}$ and the initial radio flux density increase was located in the unresolved core. The region around the core brightened as the flare progressed (Fig. 3), suggesting that new components were emerging from the core. At the end of the observations, the brightened region extended about $0.77\,{\rm mas}$ from the peak of the core, implying an average apparent velocity of $1.1\,c$ (c is the speed of light), well under the approximately $2.3\,c$ seen just beyond that distance in the first half of 2007. Astrometric results obtained as part of the VLBA monitoring program show that the position of the M 87 radio peak, relative to M 84, did not move by more than $\sim$6 $R_{\rm s}$ during the flare, suggesting that the peak emission corresponds to the nucleus of M 87.

Because VHE, X-ray and radio flares of the observed magnitude are uncommon, the fact that they happen together (chance probability of $P < 0.5\%$, supporting online text) is good evidence that they are connected. This is supported by our joint modeling of the VHE and radio light curves: The observed pattern can be explained by an event in the central region causing the VHE flare. The plasma travels down the jet and the effect of synchrotron self-absorption causes a delay of the observed peak in radio emission because the region is not transparent at radio energies at the beginning of the injection (supporting online text, Sec. 3). The VLBI structure of the flare along with the timing of the VHE activity, imply that the VHE emission occurred in a region that is small when compared with the VLBA resolution. Unless a source of infrared radiation is located very close to the central black hole, which is not supported by

current observations [30], TeV γ-ray photons can escape the central region of M 87 without being heavily absorbed through $\mathrm{e}^+\mathrm{e}^-$ pair production [19, 20].

The light curve might indicate a rise in radio flux above the range of variations observed in the past, starting before the first VHE flare was detected. This could imply that the radio emission is coming from portions of the jet launched from further out in the accretion disk than that responsible for the VHE emission. However, it is difficult to derive a quantitive statement on this, because no VHE data were taken in the week previous to the flaring. Thus, an earlier start of the VHE activity cannot be excluded, either.

A possible injection of plasma at the base of the jet observed at optical and X-ray energies with a delayed passage through the radio core $\sim 10^4\, R_\mathrm{s}$ further down the jet – interpreted as a standing shock and accompanied by an increase in radio emission – has been discussed in the case of BL Lac [9] (with evidence for VHE emission, see supporting online text for more details). M 87 is much closer than BL Lac and has a much more massive black hole, allowing the VLBA to start resolving the jet collimation region whose size, from general relativistic magnetohydrodynamic simulations [31], is thought to extend over $\sim$1000 R_s. In case of M 87 the radio core does not appear to be offset by more than the VLBA resolution of $\sim$50 R_s from the black hole (see supporting online text) and the jet has a larger angle to the line-of-sight than in BL Lac. Thus the coincidence of the VHE and radio flares (separated in photon frequency by 16 orders of magnitude), constrains the VHE emission to occur well within the jet collimation region.

Acknowledgements: *H.E.S.S.:* The support of the Namibian authorities and of the University of Namibia in facilitating the construction and operation of H.E.S.S. is gratefully acknowledged, as is the support by the German Ministry for Education and Research (BMBF), the Max Planck Society, the French Ministry for Research, the CNRS-IN2P3 and the Astroparticle Interdisciplinary Programme of the CNRS, the U.K. Science and Technology Facilities Council (STFC), the IPNP of the Charles University, the Polish Ministry of Science and Higher Education, the South African Department of Science and Technology and National Research Foundation, and by the University of Namibia. We appreciate the excellent work of the technical support staff in Berlin, Durham, Hamburg, Heidelberg, Palaiseau, Paris, Saclay, and in Namibia in the construction and operation of the equipment. *MAGIC:* The collaboration thanks the Instituto de Astrofísica de Canarias for the excellent working conditions at the Observatorio del Roque de los Muchachos in La Palma, as well as the German BMBF and MPG, the Italian INFN and Spanish MICINN. This work was also supported by ETH Research Grant TH 34/043, by the Polish MniSzW Grant N N203 390834, and by the YIP of the Helmholtz Gemeinschaft. *VERITAS:* This research is supported by grants from the U.S. Department of Energy, the U.S. National Science Foundation and the Smithsonian Institution, by NSERC in Canada, by Science Foundation Ireland and by the STFC in the U.K. We acknowledge the excellent work of the technical support staff at the FLWO and the collaborating institutions in the construction and operation of the instrument. *VLBA:* The Very Long Baseline Array is operated by the National Radio Astronomy Observatory, a facility of the U.S. National Science Foundation, operated under cooperative agreement by Associated Universities, Inc.

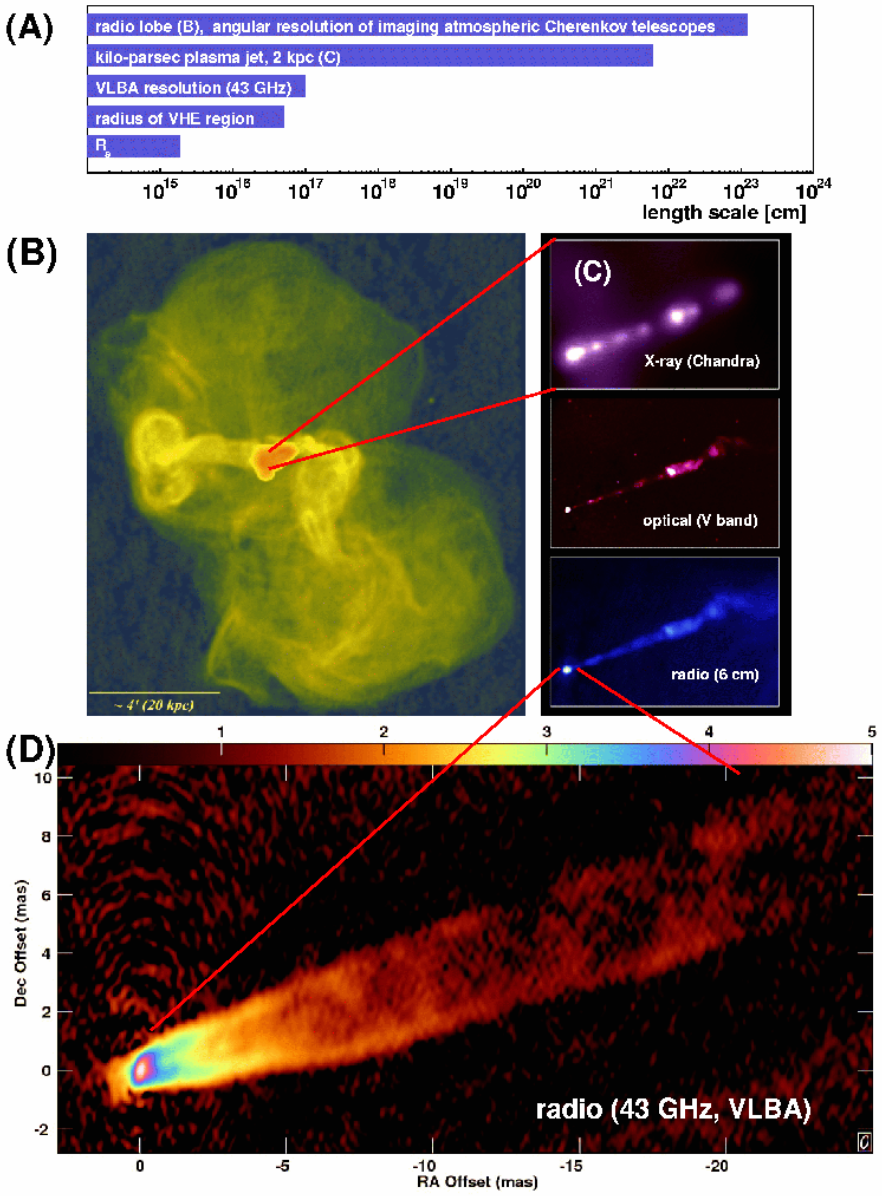

Figure 1: M 87 at different photon frequencies and length scales. (**A**): Comparison of the different length scales. (**B**): 90 cm radio emission measured with the VLA. The jet outflows terminate in a halo which has a diameter of roughly 80 kpc (15′). The radio emission in the central region is saturated in this image. Credit: F.N. Owen, J.A. Eilek and N.E. Kassim [32], NRAO/AUI/NSF. (**C**): Zoomed image of the plasma jet with an extension of 2 kpc (20″), seen in different frequency bands: X-rays (Chandra, upper panel) optical (V band, middle) and radio (6 cm, lower panel). Individual knots in the jet and the nucleus can be seen in all three frequency bands. The innermost knot HST-1 is located at a projected distance of 0.86 arcseconds (60 pc, $\approx 10^5\,R_{\rm s}$) from the nucleus. Credit: X-ray: NASA/CXC/MIT/H. Marshall et al., radio: F. Zhou, F. Owen (NRAO), J. Biretta (STScI), optical: NASA/STScI/UMBC/E. Perlman et al., [7]. (**D**): An averaged, and hence smoothed, radio image based on 23 images from the VLBA monitoring project at 43 GHz. The color scale gives the logarithm of the flux density in units of 0.01 mJy/beam. The indication of a counter-jet can be seen, emerging from the core towards the lower left side. Image from [27].

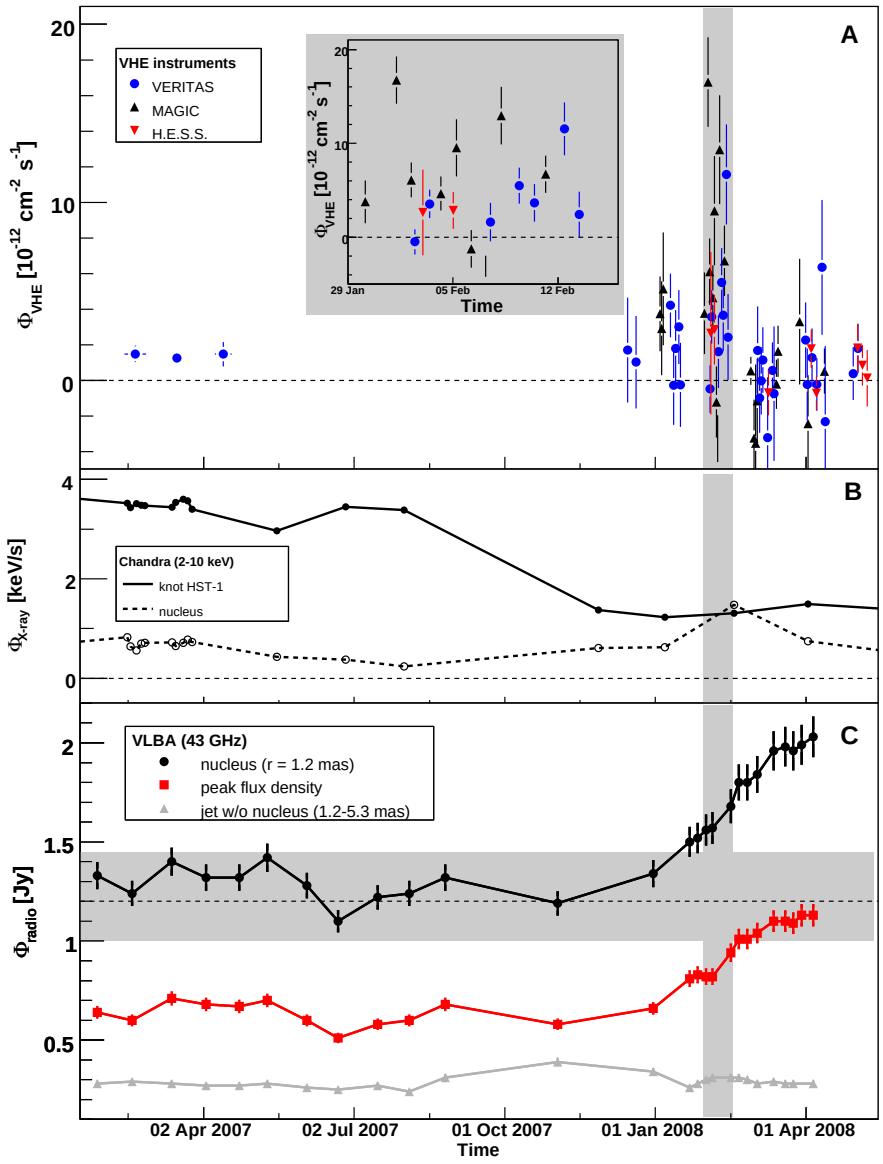

Figure 2: Combined M 87 light curves from 2007 to 2008. (**A**): VHE γ-ray fluxes ($E > 0.35\,\mathrm{TeV}$, nightly average), showing the H.E.S.S., MAGIC and VERITAS data. The fluxes with statistical errors (1 standard deviation) were calculated assuming a power-law spectral shape of $\mathrm{dN/dE} \propto \mathrm{E}^{-2.3}$. Monthly-binned archival VERITAS data taken in 2007 are also shown [4]. The systematic uncertainty in the flux calibration between the experiments was estimated to be on the order of 20% based on Crab Nebula data. The regular gaps in the light curve correspond to phases of full moon during which no observations were possible. The inlay shows a zoomed version of the flaring activity in February 2008; the time span is indicated by the grey vertical box in all panels. (**B**): Chandra X-ray measurements ($2 - 10\,\mathrm{keV}$) of the nucleus and the knot HST-1 [28]. (**C**): Flux densities from the $43\,\mathrm{GHz}$ VLBA observations are shown for (i) the nucleus (circular region with radius $r = 1.2\,\mathrm{mas} = 170\,\mathrm{R_s}$ centered on the peak flux), (ii) the peak flux (VLBA resolution element), and (iii) the flux integrated along the jet between distances of $r = 1.2 - 5.3\,\mathrm{mas}$ (compare with Fig. 3). The error bars correspond to 5% of the flux. The shaded horizontal area indicates the range of fluxes from the nucleus before the 2008 flare. Whereas the flux of the outer regions of the jet does not change substantially, most of the flux increase results from the region around the nucleus. Image from [27].

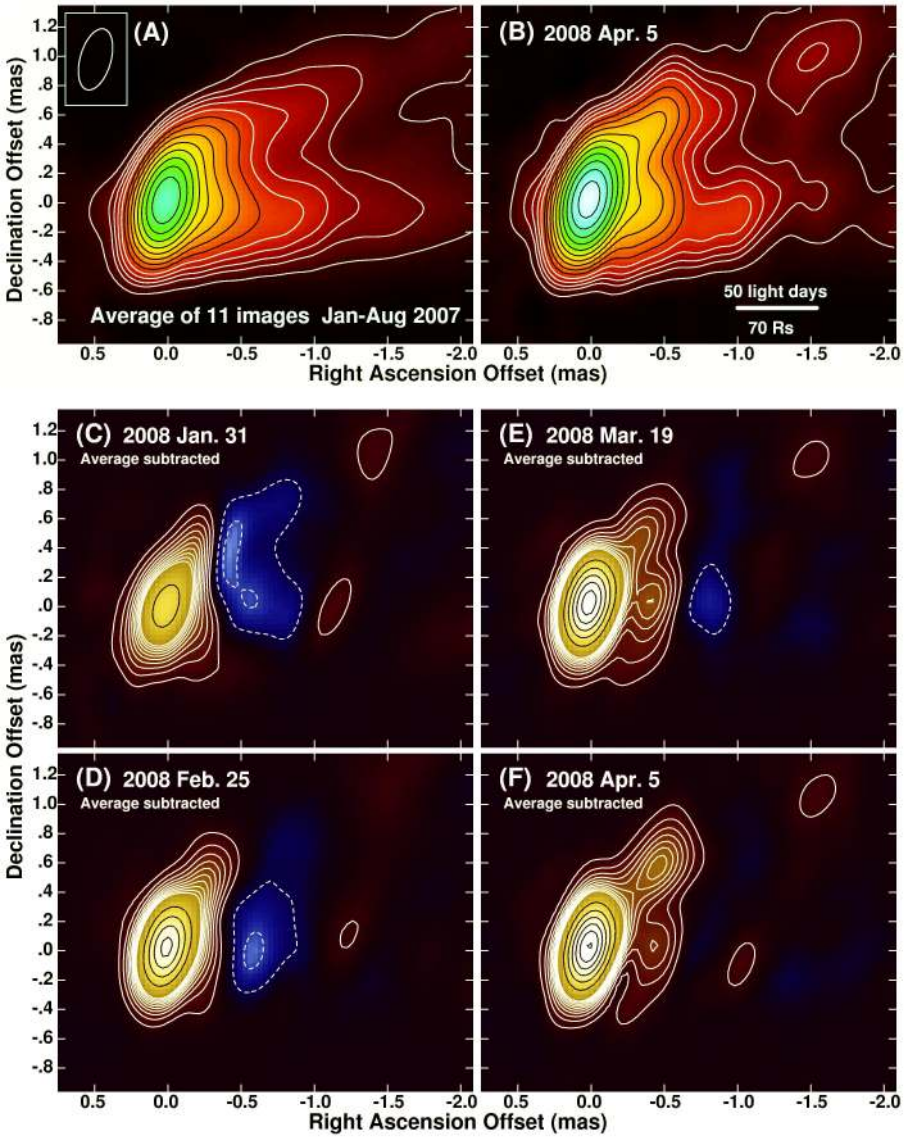

Figure 3: VLBA images of M 87 at 43 GHz. (**A**): Average (hence smoothed) of 11 images from data taken between January and August, 2007, well before the VHE and radio flare. The contour levels start at 5, 10, 14.3, and 20 mJy per beam and increase from there by factors of $\sqrt{2}$. The restoring beam used for all of the images is 0.21×0.43 mas ($30 \times 60\, R_{\rm s}$) elongated in position angle -16 deg, as shown by the ellipse in the upper left corner. (**B**): Image from 5 April 2008, with the same contours and colors as in (A). The linear scale in light days and Schwarzschild radii is also shown. (**C - F**): Difference images for observations during the period of the radio flare showing its effects. These were made by subtracting the average image (A) from the individual epoch images. The contours are linear with 10 (white) at intervals of 7 mJy per beam followed by the rest (black) at intervals of 70 mJy per beam; negative contours are indicated by dashed lines. At the time of the VHE flare, the core flux density was already above the average but the region of the jet between -0.5 and -1.0 mas RA offset was below average, suggesting that there had been a period of below-normal activity leading up to the flare and that the radio flare may have begun before the VHE flare. The sequence shows the substantial rise in the core flux density and the appearance of enhanced emission along the inner jet. Image from [27].

Supporting Online Material

1) The geometry of the M 87 jet

General assumptions. The luminosity distance of M 87 is $D = 16.7\,\mathrm{Mpc}$ [33], so that an angle of 1 milli-arc sec (mas) corresponds to $0.081\,\mathrm{pc} = 2.5 \times 10^{17}\,\mathrm{cm}$. The mass of the central black hole has been recently determined using detailed modeling of long slit spectra of the central regions of M 87 to be $(6.0 \pm 0.5) \times 10^9\,\mathrm{M}_\odot$ [6], corrected for the distance we use[2]. The Schwarzschild radius is $R_\mathrm{s} \approx 1.8 \times 10^{15}\,\mathrm{cm}$; $1\,\mathrm{mas}$ therefore corresponds to approximately $140\,R_\mathrm{s}$. The observed timing delay Δt_obs between the onset of the VHE flare and the radio peak is about $50\,\mathrm{days}$ ($\sim 4 \times 10^6\,\mathrm{s}$). The following equations hold: The observed velocity in units of the speed of light c is calculated as $\beta_\mathrm{obs} = [\beta_\mathrm{int} \sin\theta]/[1 - \beta_\mathrm{int} \cos\theta]$, the Doppler boost factor is $\delta = [\Gamma(1 - \beta_\mathrm{int} \cos\theta)]^{-1}$, the observed time delay is $\Delta t_\mathrm{obs} = \Delta t_\mathrm{int}[1 - \beta_\mathrm{int} \cos\theta)]$, and the distance along the jet is $r_\mathrm{int} = r_\mathrm{obs}/\sin\theta \approx 3\,r_\mathrm{obs}$ for $\theta = 20\,\mathrm{deg}$ (see below).

The jet orientation angle. The most rapid optical proper motions are observed along the jet with superluminal speeds [12] of $\beta_\mathrm{obs} \approx 6$ (HST-1), $\beta_\mathrm{obs} \approx 5$ (knot D), and $\beta_\mathrm{obs} \approx 4$ (knot E). On the other hand, the most rapid radio proper motions seen from features moving through HST-1 indicate superluminal speeds in the range of $\beta_\mathrm{obs} \approx 3 - 4$ [13] and through knot D indicate a superluminal speed of $\beta_\mathrm{obs} \approx 2.5$ [35]. Assuming the jet plasma moves at the speed of light ($\beta_\mathrm{int} = 1$), one obtains a maximum viewing angle of $\cos(\theta_\mathrm{max}) = [\beta_\mathrm{obs}^2 - 1]/[\beta_\mathrm{obs}^2 + 1]$. The highest optically determined superluminal speed requires a jet viewing angle of $\theta < 18.9\,\mathrm{deg}$. On the other hand, the highest radio determined superluminal speed requires $\theta < 28.0 - 36.9\,\mathrm{deg}$ for $\beta_\mathrm{obs} \approx 4 - 3$, respectively. Jet angles of $\theta = 30 - 45\,\mathrm{deg}$ were derived [10] based on radio observations at $43\,\mathrm{GHz}$, assuming the component to the East of the core is a counter-jet, and with a velocity measurement based on only one pair of observations. In this paper we assume a likely range of the jet angle of $\theta = 15 - 25\,\mathrm{deg}$.

The jet opening angle. The observations indicate the following jet full opening angles as a function of the distance to the core: $\psi_\mathrm{obs}(< 0.5\,\mathrm{mas}) \approx 60\,\mathrm{deg}$ [8], $\psi_\mathrm{obs}(1 - 5\,\mathrm{mas}) \approx 12\,\mathrm{deg}$ [26], and $\psi_\mathrm{obs}(> 10\,\mathrm{mas}) \approx 6\,\mathrm{deg}$ [11]. Assuming a jet viewing angle of $\theta = 20\,\mathrm{deg}$ the corresponding intrinsic full opening angles are: $\psi_\mathrm{int}(< 0.5\,\mathrm{mas}) \approx 30\,\mathrm{deg}$, $\psi_\mathrm{int}(1 - 5\,\mathrm{mas}) \approx 4\,\mathrm{deg}$, and $\psi_\mathrm{int}(> 10\,\mathrm{mas}) \approx 2\,\mathrm{deg}$. The observed pattern of opening angles suggest that the radio core corresponds to the formation region of the jet.

The counter-jet. The optical identification of an emission feature observed at radio frequencies located $24\,\mathrm{arc\,sec}$ away from the nucleus in the direction opposite to the jet resulted in a

[2]Gebhardt & Thomas (2009) assumed a distance of $17.9\,\mathrm{Mpc}$. As those authors point out, that mass is about 70% higher than previous determinations [34], corrected for the different assumed distances. The reason for such a large change is not fully explained yet. The use of the new mass [6] implies a higher resolution of our VLBA observations in terms of R_s, but does not substantially affect our conclusions.

first indication of a counter-jet in M 87 [36]. This feature is also seen in observations at mid-infrared frequencies [30]. Radio observations at wavelengths of $2\,\mathrm{cm}$ show clear indications of a counter-feature extending up to $3\,\mathrm{mas}$ from the radio core in the direction opposite to the jet [11]. While individual features move along the jet (determined from 21 images taken over a time span of more than 10 years), the counter feature seems to move in the opposite direction with an apparent velocity of $(0.010 \pm 0.001)\,c$, strengthening the counter-jet interpretation. However, it cannot be fully excluded that this apparent movement is a result of temporal under-sampling in the kinematic analysis, although the individual tracked jet features give consistent brightness temperatures across the observation epochs, which would be unlikely in case of incorrect cross-identifications of the components. The jet to counter-jet brightness ratio ($0.5 - 3.1\,\mathrm{mas}$) is $10 - 15$. A counter-feature is also observed at 22 and $43\,\mathrm{GHz}$, extending roughly $1\,\mathrm{mas}$ from the core in the direction opposite to the jet [10], see also Fig. 1D. The jet to counter-jet brightness ratio is calculated to be ~ 14. Marginal indication for an apparent velocity of $0.17\,c$ of the counter-jet away from the core is found from three $43\,\mathrm{GHz}$ radio images. The observations, however, suggest a temporal under-sampling of those data.

Position of the Black hole. At radio frequencies of $86\,\mathrm{GHz}$, the core is no larger than $25 \times 7\,R_\mathrm{s}$ [37], and its jet morphology is consistent with a wide-opening angle jet base, as seen at $43\,\mathrm{GHz}$, converging near the point of the black hole. Farther out between about 1 and $10\,\mathrm{mas}$ the bright edges of the jet converge toward a point close to the maximum extent of the counter-feature. Interpreting it as a part of the jet would require that the jet before the radio peak is better collimated than afterwards, although it appears to be as wide as the jet itself. The astrometric results relative to M 84 show that the root mean square scatter of the position of the radio core is about $5 \times 2\,R_\mathrm{s}$ along and across the beam with no clear systematic motion (Davies et al., in preparation). If the radio core is farther down the jet and the jet power is going up fractionally like the flux density, this would imply a very stable position of the shock region. The spatial stability is a reasonable assumption for the radio core being located close to the black hole. Theoretical modelling also supports the hypothesis that the $43\,\mathrm{GHz}$ radio peak emission results from the position of the black hole [38].

2) The VHE and radio observations and frequency of flares

VHE. The H.E.S.S., MAGIC and VERITAS collaborations operate imaging atmospheric Cherenkov telescopes (IACTs) located in Namibia, the Canary Islands (Spain) and Arizona (USA), respectively. The telescopes measure cosmic γ-ray photons (entering the atmosphere of the Earth) in an energy range of $0.1\,\mathrm{TeV}$ up to several 10's of TeV. M 87 has been observed at those energies for the last ten years. Except for the 2008 observation campaign, the observations were scheduled in advance and did not follow any external or internal triggers, leading to arbitrarily sampled light curves. During the observations of the past 10 years only two episodes of flaring activity have been measured: in 2005 [2] and in 2008 (reported in this paper). For the first time, M 87 was observed by H.E.S.S., MAGIC and VERITAS in a joint campaign for more than $120\,\mathrm{h}$

in 2008 (more than $95\,\mathrm{h}$ of data after quality selection). The integral fluxes presented in this paper (Fig. 2) were calculated[3] under the assumption that the spectrum of M 87 is described by a power-law function $\mathrm{dN/dE} \propto \mathrm{E}^{-2.3}$ [5]. Any correlation between the spectral shape and the flux level has not yet been established for M 87. The relative frequency of flaring activity was estimated by fitting the night-by-night binned light curves as measured by H.E.S.S., MAGIC and VERITAS with a constant function (using all available data – partly archival – from 2004 to 2008). Subsequently flux nights with the most significant deviation from the average were removed until the fit resulted in a reduced χ^2 per degree of freedom of less than 1; all removed points corresponded to flux values higher than the average. The light curves are compatible with constant emission for 49 out of 53 nights (H.E.S.S., 2004-2008), 12 out of 21 nights (MAGIC, 2008) and 50 out of 51 nights (VERITAS, 2007-2008). Combining these numbers one finds flaring activity in the so far recorded data in 14 out of 125 nights of observations, resulting in a relative frequency of flares on the order of 10% of all observed nights. Almost all data were recorded arbitrarily and except for four nights (with a time difference of $\sim 0.5\,\mathrm{days}$ between the VERITAS and the H.E.S.S./MAGIC observations) all observations were separated in time by more than one day. Therefore we assume that this number gives an estimate of the general chance to measuring a VHE γ-ray flare from M 87. However, the relative frequency of flaring activity is overestimated by the fact that the 2008 observations were intensified for some nights during the high flux state following the VHE trigger by MAGIC [5].

X-ray. M 87 was regularly observed at X-ray energies with Chandra, resulting in 61 measurements of the X-ray flux of the nucleus during the last ten years [28]. Three measurements exceed a flux level higher than 2 times the root mean square (RMS) of the average flux of all data points (relative occurrence of $\sim 5\%$). Only one measurement exceeds the level of $3\,\mathrm{RMS}$ which was taken during the radio flare with a deviation of $\sim 4.3\,\mathrm{RMS}$ (Fig. 2 in the main text).

Radio. Throughout 2007, M 87 was observed with the VLBA on a regular basis roughly every three weeks [39]. The aim of this 'movie project' was to study morphological changes of the plasma jet with time. Preliminary analysis of the first 7 months showed a fast evolving structure, somewhat reminiscent of a smoke plume, with apparent velocities of about twice the speed of light. These motions were faster than expected so the movie project was extended from January to April 2008 with a sampling interval of 5 days. A full analysis of these data is in progress and details will be published elsewhere. The observed radio flux densities reached at the end of the 2008 observations, roughly 2 months after the VHE flare occurred, are larger than seen in any previous VLBI observations of M 87 at this frequency, including during the preceding 12 months of intensive monitoring, in 6 observations in 2006 and in individual observations in 1999, 2000, 2001, 2002, and 2004 [10]. The MOJAVE project web site[4] gives $15\,\mathrm{GHz}$ VLBA

[3] the H.E.S.S. flux points – measured with a higher energy threshold – were extrapolated down from $\sim 1\,\mathrm{TeV}$.
[4] http://www.physics.purdue.edu/MOJAVE/

flux densities at 27 epochs since 1995, with the highest flux value measured on May 1, 2008[5]; most of the data (except the last two epochs) are published in [40]. Assuming a flare duration of $\sim$4 months, a similar flare was not observed during a total period of $5 \times 4 = 20$ months based on the 5 observations from 2004 and earlier, which are well separated, 8 months taking into account overlap based on the 2006 pilot observations spread over 4 months, and 14 months during the 2007/2008 monitoring including 2 months before the start but not including the time during the observed flare. That is 42 months total for which a similar flare was not in progress. By the same accounting, there are 4 months with a flare. So the probability of a radio flare being in progress at any given time is $4/46 \approx 10\%$, suggesting that radio flares of the observed magnitude are uncommon.

The observed radio/X-ray/VHE-pattern. The probability of observing k out of n nights exceeding a flux baseline (for which the chance probability is p) is: $p(n,k) = \binom{n}{k} \cdot p^k \cdot (1-p)^{n-k}$. The probability of observing k or more flare nights is $P(n, \geq k) = \sum_{j=k}^{n} p(n,j)$. A joint estimated of the chance probability of the observed pattern is difficult, since the characteristic time scales of flux changes are different and the data are not sampled equally, or are partly sampled with higher frequencies as the characteristic time scale of the flux changes (over-sampling) or much less frequent (under-sampling). However, if defining a time window covering the whole increase of the radio flux between end of January to mid of April one finds 8 out of 40 VHE measurements ($P_{\rm VHE}$) and 1 out of 2 X-ray measurements ($P_{\rm X-ray}$) exceeded their baselines. The chance probability of observing this pattern during the radio flare is on the order of $P = P_{\rm VHE} \cdot P_{\rm X-ray} = 0.026 \cdot 0.095 < 0.5\%$. The fluxes in the radio, X-ray, and VHE bands reached their highest archival level during the defined time window.

3) Time-dependent modelling of the radio emission as synchrotron emission from a slow outer sheath

The model. Whereas the VHE γ-ray emission from M 87 varies on time scales of a few days, the $43\,{\rm GHz}$ radio emission from the nucleus steadily increases over a time period of two months (Fig. 2). A model calculation was performed to test if the slow variations of the radio flux can be explained with a self-absorbed synchrotron model of electrons injected into a "slow outer sheath" of jet plasma. The slow outer sheath has the geometry of a hollow cone, an assumption which is supported by the edge-brightened structure of the jet observed at radio frequencies (Fig. 1D). As the plasma travels down the jet, it expands, leading to a decline of the frozen-in magnetic field and to adiabatic cooling of the electrons. In the model, a γ-ray flare leads to the injection of radio-emitting plasma at the base of the jet and at the base of the slow outer sheath. The model assumes that the VHE γ-rays are produced very close to the black hole, e.g. in the black hole magnetosphere and does not attempt to describe the production mechanism. It merely

[5]This is only a few weeks later than the maximum of the $43\,{\rm GHz}$ flux reported in this paper. However, no further $15\,{\rm GHz}$ data for 2008 are listed on the MOJAVE web page.

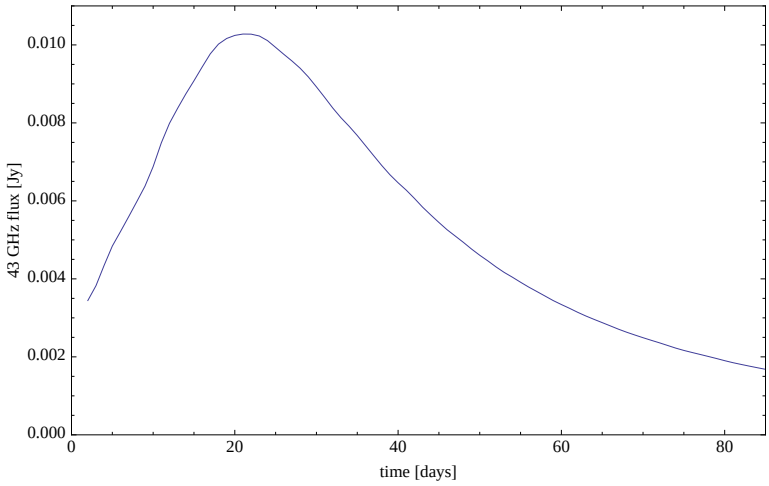

Figure 4: Simulated $43\,\mathrm{GHz}$ light curve resulting from a single injection of radio-emitting plasma at time $t = 0$ ($\Gamma = 1.01$, $\beta_{\rm jet} = 0.14$, $B = 0.5\,\mathrm{G}$). Initially, the plasma is opaque owing to synchrotron self-absorption. As the plasma travels away from the point of injection, it expands and becomes transparent. The expansion leads to a decrease of the magnetic field and to adiabatic cooling of the electrons, and thus to the decline of the radio emission. The small deviations during the injection stage are due to numerical effects.

uses the observed γ-ray fluxes to normalize the energy spectrum of the electrons responsible for the radio emission. In the beginning, the radio-emitting plasma is optically thick, and the synchrotron emission cannot escape. Owing to the adiabatic expansion, the plasma eventually becomes optically thin leading to a radio flare. The radio flare dies down owing to the decline of the magnetic field and the adiabatic cooling of the electrons.

Following the injection of radio-emitting plasma at time t_0, a ring of plasma with radius $R = R_{\rm s} + \beta_{\rm jet} c \sin\alpha (t - t_0)$ (with the thickness of the radio bright sheath being 1/5th of the cone radius) travels down the jet. The emission of the ring is computed in the frame of the moving plasma, assuming that the magnetic field scales as $B \propto 1/R$, and the electrons cool adiabatically. The calculation uses the standard equations for Lorentz transforming the emission of different sections of the ring, see for example [41]. Taking into account light travel time effects, the received radio flux at $43\,\mathrm{GHz}$ is computed. The overall normalization of the electron energy spectrum is adjusted to reproduce the observed radio flux. The results of the model strongly depend on the choice of the minimal radius $R_{\rm min} = R_{\rm s}$, and weakly depend on the choices of the magnetic field B, the jet opening angle α, and and the thickness of the sheath.

Results. We assume an intrinsic cone opening angle of $\alpha = 5\,\mathrm{deg}$, a jet angle of $\theta = 20\,\mathrm{deg}$ and a rather low magnetic field of $B = 0.5\,\mathrm{G}$ at the base of the jet for which radiative cooling can be neglected. The simulated radio light curve produced by a single injection of radio-emitting plasma is shown in Fig. 4 for an assumed bulk Lorentz factor of $\Gamma = 1.01$ ($\beta_{\rm jet} = 0.14$, giving the best fit result). The radio flux needs approximately 20 days to reach its maximum. Figure 5 shows the corresponding radio light curve obtained when choosing a time-dependent electron injection function proportional to the measured VHE γ-ray fluxes, starting with the VHE data taken in January 2008. The spatial extent of the predicted radio source after 50 days is ~ 3 light days and therefore still within the central resolution element of the VLBA observations (Fig. 3). The model was chosen to minimize the number of free parameters and assumptions. Other dependencies could affect the results as follows: (i) If the emitting plasma is more compact (and

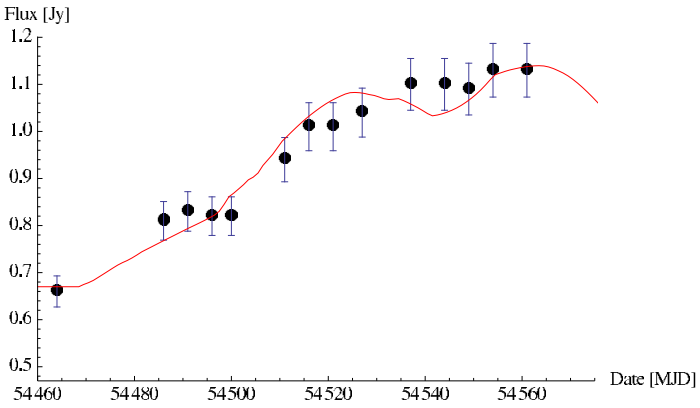

Figure 5: Observed (data points) and modelled (line) 43 GHz radio flux. The modelled curve was obtained by using the measured VHE γ-ray light curve as source function for injecting radio-emitting plasma into the slow sheath of the jet. The Bulk Lorentz factor used is $\Gamma = 1.01$ ($\beta_{\rm jet} = 0.14$). No VHE γ-ray observations were possible during phases of full moon, leaving some uncertainties for the injection function.

the volume filling factor is < 1), it stays synchrotron self-absorbed for a longer time, increasing the time lag between the γ-ray flares and the rise of the radio flux. (ii) The emission volume may expand slower than proportional to t^2, as assumed in the model. Slower expansion would slow down the time scale for the rise and decay of the radio flux. (iii) A higher value of $\beta_{\rm jet}$ would result in a faster radio flare. (iv) All non-thermal particles are injected into the jet right at the base of the slow sheath. This model assumption may not be accurate. Additional non-thermal particles may be accelerated further downstream which would lead to a longer duration of the radio flare. (v) If the magnetic field at the base of the jet is stronger, radiative cooling is not negligible any longer and fitting the data would require an assumption of continued acceleration as the outer shell flows down the jet. (vi) In a turbulent jet flow, efficient stochastic re-acceleration may occur, which could change the picture. However, the current model calculations show that synchrotron self-absorption may play a role in explaining the observed slower turn-on of the radio emission.

4) Investigation of VHE γ-ray models for the M 87 VHE/radio flare

The key questions for the understanding of the VHE γ-ray emission measured from the radio galaxy M 87 and from the more than 20 known VHE γ-ray blazars are: (i) What is the underlying particle distribution which is accelerated, (ii) what are the mechanisms to generate the γ-rays, and (iii) where is the region of the emission located. In the following paragraphs a selection of models discussed for M 87 in the literature is investigated with a focus on the question whether they can explain the observed VHE/radio light curves. Note, however, that some of the models have difficulties in explaining the observed hard VHE γ-ray spectra [2, 5], which will however not be discussed in more detail.

4.1) Black hole magnetosphere models

Models of VHE emission from the black hole magnetosphere. The electromagnetic mechanism of extraction of the rotational energy of black holes by the Blandford & Znajek scenario

[42] seems to be a viable mechanism for powering the relativistic jets of AGN. Particles can be accelerated by the electric field of vacuum gaps in the black hole magnetosphere [19] (the electric field component parallel to the ordered magnetic field is not screened out) or due to centrifugal acceleration in an active plasma-rich environment, where the parallel electric field is screened [20]. Synchrotron and curvature radiation of the charged particles, and inverse Compton scattering of thermal photons can produce VHE γ-ray photons [43]. An important question in this scenario is if the γ-rays can escape the central region or if they are absorbed through pair creation processes with either photons from the accretion disk [13] or infrared photons emitted by a potential dust torus for which no clear observational evidence is found so far [30, 44]. If M 87 harbours a non-standard (advection-dominated) accretion disk, γ-rays could escape without being absorbed [20]. An alternative scenario could be that the primary photons create a pair cascade whose leakage produces the observed γ-ray emission [45]. The delayed radio emission could be explained by the effect of synchrotron self-absorption (see Sec. 3) or the time needed to cool the electrons before they dominantly emit synchrotron radiation in the radio regime.

4.2) Hadronic jet models

The model of Reimer et al. (2004). In this model a primary relativistic electron population is injected together with high-energy protons into a highly magnetized emission region [18]. The VHE emission is dominated by either $\mu^{\pm}/\pi^{\pm}$ synchrotron radiation or by proton synchrotron radiation. The low-energy component is explained by the synchrotron emission of the electron population. However, the radio flux is underestimated by the (steady-state) model (explanations are discussed in the paper) so that a discussion of the observed radio/VHE flare is beyond the scope of this particular model.

4.3) Leptonic jet models

The model of Lenain et al. (2008). In this model the high-energy emission region (X-rays up to VHE) consists of small blobs ($\sim 10^{14}\,\mathrm{cm}$) travelling through the extended jet and radiating at distances just beyond the Alfven surface [17]. The emission takes place in the broadened jet formation region, in the innermost part of the jet (corresponding to the central resolution element in the $43\,\mathrm{GHz}$ radio map). This multi-blob model is a two-flow model, where the fast, compact blobs contribute to X-rays and γ-rays through the synchrotron self-Compton mechanism, and are embedded in an extended, diluted and slower jet emitting synchrotron radiation from radio to optical frequencies. Even though this model describes only steady state emission, the observed radio/VHE variability can be discussed qualitatively. For instance, a sudden rise of the density of the underlying leptonic population at the stationary shock (i.e. in the blobs) translates into a flare of X-rays and γ-rays, but no immediate rise of radio emission is expected, because the emission volume is synchrotron self-absorbed at radio frequencies, see Sec. 3. However, as the flare propagates into the extended, less magnetized, neighbouring jet, the leptons in the jet are energized and could cool by emitting at radio frequencies with some delay, creating a di-

luted radio flare in response to the VHE flare. An alternative scenario by Giannios et al. (2009) explains the fast variability of VHE γ-ray radiation in blazars as a possible result from large Lorentz factor (100) filaments within a more slowly moving jet flow [46].

The model of Tavecchio and Ghisellini (2008). According to this model [21] the jet consists of a fast spine and slow sheath layer. The photons from the fast spine are external-Compton boosted to VHE by the slower sheath. In this framework one may assume that the VHE flare comes from near to the core and the time lag to the radio maximum is entirely a result of propagation of some disturbance down the jet and the associated reduction in synchrotron self-absorption. The X-rays should be synchrotron emission that is not self-absorbed and flare at about the same time as the VHE γ-rays. In the radio data we see significant edge brightening suggestive of a de-boosted spine. Note, however, that edge brightening like that observed can also be produced by enhanced surface emissivity. In the model the radio emission originates from a region different from that producing the VHE emission, so that a strict flux correlation is not required. Detailed modeling would be needed to explain the observed light curves in the framework of this model.

The model of Georganopoulos et al. (2005). In this model the jet decelerates over a length of $0.1\,\mathrm{pc} = 3 \cdot 10^{17}\,\mathrm{cm}$ [16]. The VHE emission is assumed to come from the fast moving part near the jet base by inverse-Compton scattering of low-frequency photons from the slower moving part of the jet. The model calculations are steady state so that they are difficult to apply to an ejection event. However, one can assume that the VHE flare is directly associated with the ejection event. As the disturbance propagates down the jet and decelerates we see the radio rise later as a result of synchrotron self-absorption effects, similar to the model described in Sec. 3. Here the X-ray flux can still rise and fall with the VHE if it comes directly from the disturbance; the majority of the observed power comes from the slower part of the flow, but this is a more or less steady state result. A similar model by Levinson (2007) of radiative decelerating blobs in the jets of VHE γ-ray emitting blazars is described in [47].

4.4) Jet base / standing shock models

The model of Marscher et al. (2008). The model is based on the observation of a double flare in BL Lac [9]. The first flare is seen at X-ray/optical energies accompanied by polarization measurements at a date of 2005.82. It indicates an injection event into the jet acceleration and collimation region near to the black hole. The flare was followed by the appearance of a new radio component in VLBA images that approached and passed through the radio core, accompanied by a second X-ray/optical flare at 2005.92, where the $14.5\,\mathrm{GHz}$ radio flux begins to increase and peaks at about 2006.0. This is interpreted as the passage of the disturbance through a standing shock in the jet at a distance of $\sim 10^4\,R_\mathrm{s}$, see Fig. 3 in [9]. VHE γ-ray emission has been detected in 2005, however, no evidence for flux variability has been found in the data. In this picture the radio core is located at the standing shock and the radio emission in the

acceleration and collimation region may be (i) either intrinsically weak or (ii) synchrotron self-absorbed. The non-coincidence between the radio peak and the second peak in the X-ray/optical is proposed to arise from the longer lifetime of particles radiating at radio frequencies. Since the disturbance passes down the expanding jet the radio emission might last longer than the second X-ray/optical flare but does not increase in strength after the disturbance passes through the shock.

Applying this model to M 87 one can assume that the observed VHE flare corresponds to (A) the first or (B) the second flare. A: The VHE flare indicates the injection at the base of the jet and the increase of the radio flux corresponds to the passage through a standing shock that is located at the M 87 radio core. In this case, the counter-feature would have to be interpreted as the jet before the standing shock. Although the peak of the radio emission is delayed, the radio flux started to increase at about the same time as the VHE flare, which indicates that the two emission regions are not spatially separated, making this scenario unlikely. B: The VHE flare indicates the passage of the disturbance through the standing shock accompanied by a slow increase of the radio flux. In this interpretation the first flare related to the injection at the base of the jet would have been missed completely in any of the wavelengths. There would still be a problem with a non time coincident maximum in the VHE and radio emission. The VHE to radio lag could be explained by synchrotron self-absorption (see Sec. 3.), which would seem to require a coincidental juxtaposition of the standing shock with just the right radio optical depth and subsequent optical depth decline down the expanding jet. An alternative scenario could be that the shock-accelerated particles causing the VHE emission cool rapidly until they later emit photons dominantly at radio frequencies.

BL Lac is 16 times farther away than M 87, and the jet angle is considerably smaller ($\theta \approx 7\,\mathrm{deg}$) as compared to M 87. The black hole in M 87, on the other hand, is ~ 30 times more massive than the one in BL Lac. Therefore, our data have a ~ 16 times higher spatial resolution[6] and provide a more than two orders of magnitude more detailed insight into the jet physics on gravitational scales: In case of the M 87 observations presented here, $1\,\mathrm{mas}$ corresponds to $140\,R_\mathrm{s}$, whereas in the case of the BL Lac observations, $1\,\mathrm{mas}$ corresponds to $\sim 70,000\,R_\mathrm{s}$. Although the Marscher et al. model makes use of the observed VHE emission in BL Lac, there is no experimental evidence that would constrain the spatial region of that emission. Our observations connect the VHE emission with the radio emission from the nucleus in M 87 and therefore contrain the VHE emission region to lie within the collimation region of the jet, at maximum a few hundred R_s away from the black hole.

References and Notes

[1] J.A. Gaidos, *et al.*, *Nature* **383**, 319-320 (1996).

[2] F. Aharonian, *et al.* (H.E.S.S. Collaboration), *Science* **314**, 1424-1427 (2006).

[3] F. Aharonian, *et al.* (HEGRA Collaboration), *A&A* **403**, L1-L5 (2003).

[6] even though the observations in [9] use an angular resolution twice as high as ours at $43\,\mathrm{GHz}$

[4] V.A. Acciari, *et al.* (VERITAS Collaboration), *ApJ* **679**, 397-403 (2008).
[5] J. Albert, *et al.* (MAGIC Collaboration), *ApJ* **685**, L23-L26 (2008).
[6] K. Gebhardt, & J. Thomas, *accepted by ApJ*, see arXiv:0906.1492 (2009).
[7] A.S. Wilson, & Y. Yang, *ApJ* **568**, 133-140 (2002).
[8] W. Junor, J.A. Biretta, & M. Livio, *Nature* **401**, 891-892 (1999).
[9] A.P. Marscher, *et al.*, *Nature* **452**, 966-969 (2008).
[10] C. Ly, R.C. Walker, & W. Junor, *ApJ* **660**, 200-205 (2007).
[11] Y.Y. Kovalev, M.L. Lister, D.C. Homan, & K.I. Kellermann, *ApJ* **668**, L27-L30 (2007).
[12] J.A. Biretta, W.B. Sparks, & F. Macchetto, *ApJ* **520**, 621-626 (1999).
[13] C.C. Cheung, D.E. Harris, & L. Stawarz, *ApJ* **663**, L65-L68 (2007).
[14] E.A. Baltz, *et al.*, *PhRvD* **61**, 023514 (2000).
[15] C. Pfrommer, & T.A. Enßlin, *A&A* **407**, L73-L77 (2003).
[16] M. Georganopoulos, E.S. Perlman, & D. Kazanas, *ApJ* **634**, L33-L36 (2005).
[17] J.-P. Lenain, *et al.*, *A&A* **478**, 111-120 (2008).
[18] A. Reimer, R.J. Protheroe, & A.-C. Donea, *A&A* **419**, 89-98 (2004).
[19] A. Neronov, & F.A. Aharonian, *ApJ* **671**, 85-96 (2007).
[20] F.M. Rieger, & F.A. Aharonian, *IJMPD* **17**, 1569-1575 (2008).
[21] F. Tavecchio, & G. Ghisellini, *MNRAS* **385**, L98-L102 (2008).
[22] F. Aharonian, *et al.* (H.E.S.S. Collaboration), *A&A* **457**, 899-915 (2006).
[23] J. Albert, *et al.* (MAGIC Collaboration), *ApJ* **674**, 1037-1055 (2008).
[24] V.A. Acciari, *et al.* (VERITAS Collaboration), *ApJ* **679**, 1427-1432 (2008).
[25] P.J. Napier, D.S. Bagri, B.G. Clark, et al., *Proc. IEEE* **82**, 658 (1994).
[26] R.C. Walker, C. Ly, W. Junor, & P.E. Hardee, *Eds. Astronomical Society of the Pacific Conference Series* (Y. Hagiwara and E. Fomalont and M. Tsuboi and Y. Murata 2008), *Preprint: arXiv:0803.1837*.
[27] V. Acciari, *et al.*, *Science* **325**, 444 (2009), DOI: 10.1126/science.1175406, see *http://www.sciencemag.org/cgi/content/abstract/sci;325/5939/444*.
[28] D.E. Harris, C.C. Cheung, & L. Stawarz, *ApJ* **699**, 305-314 (2009).
[29] D.E. Harris, *et al.*, *ApJ* **640**, 211-218 (2006).
[30] E.S. Perlman, R.E. Mason, C. Packham, N.A. Levenson, *et al.*, *ApJ* **663**, 808-815 (2007).
[31] J.C. McKinney, *MNRAS* **368**, 1561-1582 (2006).
[32] F.N. Owen, J.A. Eilek, & N.E. Kassim, *ApJ* **543**, 611-619 (2000).
[33] S. Mei et al., *ApJ* **655**, 144-162 (2007).
[34] F. Macchetto, A. Marconi, D.J. Axon, et al., *ApJ* **489**, 579 (1997).
[35] J.A. Biretta, F. Zhou, & F.N. Owen, *ApJ* **447**, 582-596 (1995).
[36] W.B. Sparks, D. Fraix-Burnet, F. Macchetto, & F.N. Owen, *Nature* **355**, 804-806 (1992).
[37] T.P. Krichbaum, *et al.*, *Journal of Physics: Conference Series* **54**, 328-334 (2006).
[38] A.E. Broderick, & A. Loeb, *ApJ* **697**, 1164-1179 (2009).
[39] R.C. Walker, C. Ly, W. Junor, & P.E. Hardee, *JPhCS* **131**, pp.012053 (2008).

[40] M.L. Lister, *et al.*, *AJ* **137**, 3718-3729 (2009).
[41] G.B. Rybicki, & A.P. Lightman, *ApJ* **232**, 882-890 (1979).
[42] R.D. Blandford, & R.L. Znajek, *MNRAS* **179**, 433-456 (1977).
[43] H. Krawczynski, *ApJ* **659**, 1063-1073 (2007).
[44] D. Whysong, & R. Antonucci, *ApJ* **602**, 116-122 (2004).
[45] W. Bednarek, *MNRAS* **285**, 69-81 (1997).
[46] D. Giannios, D. Uzdensky, & M.C. Begelman, *MNRAS*, **395**, L29-L33 (2009).
[47] A. Levinson, *ApJ* **671**, L29-L32 (2007).

Full list of authors

The VERITAS Collaboration: V. A. Acciari[1], E. Aliu[2], T. Arlen[3], M. Bautista[4], M. Beilicke[5], W. Benbow[1], S. M. Bradbury[6], J. H. Buckley[5], V. Bugaev[5], Y. Butt[7], K. Byrum[8], A. Cannon[9], O. Celik[3], A. Cesarini[10], Y. C. Chow[3], L. Ciupik[11], P. Cogan[4], W. Cui[12], R. Dickherber[5], S. J. Fegan[3], J. P. Finley[12], P. Fortin[13], L. Fortson[11], A. Furniss[14], D. Gall[12], G. H. Gillanders[10], J. Grube[9], R. Guenette[4], G. Gyuk[11], D. Hanna[4], J. Holder[2], D. Horan[15], C. M. Hui[16], T. B. Humensky[17], A. Imran[18], P. Kaaret[19], N. Karlsson[11], D. Kieda[16], J. Kildea[1], A. Konopelko[20], H. Krawczynski[5], F. Krennrich[18], M. J. Lang[10], S. LeBohec[16], G. Maier[4], A. McCann[4], M. McCutcheon[4], J. Millis[21], P. Moriarty[22], R. A. Ong[3], A. N. Otte[14], D. Pandel[19], J. S. Perkins[1], D. Petry[23], M. Pohl[18], J. Quinn[9], K. Ragan[4], L. C. Reyes[24], P. T. Reynolds[25], E. Roache[1], E. Roache[1], H. J. Rose[6], M. Schroedter[18], G. H. Sembroski[12], A. W. Smith[8], S. P. Swordy[17], M. Theiling[1], J. A. Toner[10], A. Varlotta[12], S. Vincent[16], S. P. Wakely[17], J. E. Ward[9], T. C. Weekes[1], A. Weinstein[3], D. A. Williams[14], S. Wissel[17], M. Wood[3]

The VLBA 43 GHz M87 Monitoring Team: R.C. Walker[26], F. Davies[26,27], P.E. Hardee[28], W. Junor[29], C. Ly[30]

The H.E.S.S. Collaboration: F. Aharonian[31,43], A.G. Akhperjanian[32], G. Anton[46], U. Barres de Almeida[38,60], A.R. Bazer-Bachi[33], Y. Becherini[42], B. Behera[44], K. Bernlöhr[31,35], A. Bochow[31], C. Boisson[36], J. Bolmont[49], V. Borrel[33], J. Brucker[46], F. Brun[49], P. Brun[37], R. Bühler[31], T. Bulik[54], I. Büsching[39], T. Boutelier[47], P.M. Chadwick[38], A. Charbonnier[49], R.C.G. Chaves[31], A. Cheesebrough[38], L.-M. Chounet[40], A.C. Clapson[31], G. Coignet[41], M. Dalton[35], M.K. Daniel[38], I.D. Davids[52,39], B. Degrange[40], C. Deil[31], H.J. Dickinson[38], A. Djannati-Ataï[42], W. Domainko[31], L.O'C. Drury[43], F. Dubois[41], G. Dubus[47], J. Dyks[54], M. Dyrda[58], K. Egberts[31], D. Emmanoulopoulos[44], P. Espigat[42], C. Farnier[45], F. Feinstein[45], A. Fiasson[45], A. Förster[31], G. Fontaine[40], M. Füßling[35], S. Gabici[43], Y.A. Gallant[45], L. Gérard[42], D. Gerbig[51], B. Giebels[40], J.F. Glicenstein[37], B. Glück[46], P. Goret[37], D. Göhring[46], D. Hauser[44], M. Hauser[44], S. Heinz[46], G. Heinzelmann[34], G. Henri[47], G. Hermann[31], J.A. Hinton[55], A. Hoffmann[48], W. Hofmann[31], M. Holleran[39], S. Hoppe[31], D. Horns[34], A. Jacholkowska[49], O.C. de Jager[39], C. Jahn[46], I. Jung[46], K. Katarzyński[57], U. Katz[46], S. Kaufmann[44], E. Kendziorra[48], M. Kerschhaggl[35], D. Khangulyan[31], B. Khélifi[40], D. Keogh[38], W. Kluźniak[54], T. Kneiske[34], Nu. Komin[37], K. Kosack[31], G. Lamanna[41], J.-P. Lenain[36], T. Lohse[35], V. Marandon[42], J.M. Martin[36], O. Martineau-Huynh[49], A. Marcowith[45], D. Maurin[49], T.J.L. McComb[38], M.C. Medina[36], R. Moderski[54],

E. Moulin[37], M. Naumann-Godo[40], M. de Naurois[49], D. Nedbal[50], D. Nekrassov[31], B. Nicholas[56], J. Niemiec[58], S.J. Nolan[38], S. Ohm[31], J-F. Olive[33], E. de Oña Wilhelmi[42,59], K.J. Orford[38], M. Ostrowski[53], M. Panter[31], M. Paz Arribas[35], G. Pedaletti[44], G. Pelletier[47], P.-O. Petrucci[47], S. Pita[42], G. Pühlhofer[44], M. Punch[42], A. Quirrenbach[44], B.C. Raubenheimer[39], M. Raue[31,59], S.M. Rayner[38], M. Renaud[42,31], F. Rieger[31,59], J. Ripken[34], L. Rob[50], S. Rosier-Lees[41], G. Rowell[56], B. Rudak[54], C.B. Rulten[38], J. Ruppel[51], V. Sahakian[32], A. Santangelo[48], R. Schlickeiser[51], F.M. Schöck[46], R. Schröder[51], U. Schwanke[35], S. Schwarzburg[48], S. Schwemmer[44], A. Shalchi[51], M. Sikora[54], J.L. Skilton[55], H. Sol[36], D. Spangler[38], Ł. Stawarz[53], R. Steenkamp[52], C. Stegmann[46], F. Stinzing[46], G. Superina[40], A. Szostek[53,47], P.H. Tam[44], J.-P. Tavernet[49], R. Terrier[42], O. Tibolla[31,44], M. Tluczykont[34], C. van Eldik[31], G. Vasileiadis[45], C. Venter[39], L. Venter[36], J.P. Vialle[41], P. Vincent[49], M. Vivier[37], H.J. Völk[31], F. Volpe[31,40,59], S.J. Wagner[44], M. Ward[38], A.A. Zdziarski[54], A. Zech[36],

The MAGIC Collaboration: H. Anderhub[61], L. A. Antonelli[62], P. Antoranz[63], M. Backes[64], C. Baixeras[65], S. Balestra[63], J. A. Barrio[63], D. Bastieri[66], J. Becerra González[67], J. K. Becker[64], W. Bednarek[68], K. Berger[68], E. Bernardini[69], A. Biland[61], R. K. Bock[70,66], G. Bonnoli[71], P. Bordas[72], D. Borla Tridon[70], V. Bosch-Ramon[72], D. Bose[63], I. Braun[61], T. Bretz[73], I. Britvitch[61], M. Camara[63], E. Carmona[70], S. Commichau[61], J. L. Contreras[63], J. Cortina[74], M. T. Costado[67,75], S. Covino[62], V. Curtef[64], F. Dazzi[76,85], A. De Angelis[76], E. De Cea del Pozo[77], C. Delgado Mendez[67], R. De los Reyes[63], B. De Lotto[76], M. De Maria[76], F. De Sabata[76], A. Dominguez[78], D. Dorner[61], M. Doro[66], D. Elsaesser[73], M. Errando[74], D. Ferenc[79], E. Fernández[74], R. Firpo[74], M. V. Fonseca[63], L. Font[65], N. Galante[70], R. J. García López[67,75], M. Garczarczyk[74], M. Gaug[67], F. Goebel[70,86], D. Hadasch[65], M. Hayashida[70], A. Herrero[67,75], D. Hildebrand[61], D. Höhne-Mönch[73], J. Hose[70], C. C. Hsu[70], T. Jogler[70], D. Kranich[61], A. La Barbera[62], A. Laille[79], E. Leonardo[71], E. Lindfors[80], S. Lombardi[66], F. Longo[76], M. López[66], E. Lorenz[61,70], P. Majumdar[69], G. Maneva[81], N. Mankuzhiyil[76], K. Mannheim[73], L. Maraschi[62], M. Mariotti[66], M. Martínez[74], D. Mazin[74], M. Meucci[71], J. M. Miranda[63], R. Mirzoyan[70], H. Miyamoto[70], J. Moldón[72], M. Moles[78], A. Moralejo[74], D. Nieto[63], K. Nilsson[80], J. Ninkovic[70], I. Oya[63], R. Paoletti[71], J. M. Paredes[72], M. Pasanen[80], D. Pascoli[66], F. Pauss[61], R. G. Pegna[71], M. A. Perez-Torres[78], M. Persic[76,82], L. Peruzzo[66], F. Prada[78], E. Prandini[66], N. Puchades[74], I. Reichardt[74], W. Rhode[64], M. Ribó[72], J. Rico[83,74], M. Rissi[61], A. Robert[65], S. Rügamer[73], A. Saggion[66], T. Y. Saito[70], M. Salvati[62], M. Sanchez-Conde[78], K. Satalecka[69], V. Scalzotto[66], V. Scapin[76], T. Schweizer[70], M. Shayduk[70], S. N. Shore[84], N. Sidro[74], A. Sierpowska-Bartosik[77], A. Sillanpää[80], J. Sitarek[70,68], D. Sobczynska[68], F. Spanier[73], A. Stamerra[71], L. S. Stark[61], L. Takalo[80], F. Tavecchio[62], P. Temnikov[81], D. Tescaro[74], M. Teshima[70], D. F. Torres[83,77], N. Turini[71], H. Vankov[81], R. M. Wagner[70], V. Zabalza[72], F. Zandanel[78], R. Zanin[74], J. Zapatero[65].

[1]*Fred Lawrence Whipple Observatory, Harvard-Smithsonian Center for Astrophysics, Amado, AZ 85645, USA*, [2]*Department of Physics and Astronomy and the Bartol Research Institute, University of Delaware, Newark, DE 19716, USA*, [3]*Department of Physics and Astronomy, University of California, Los Angeles, CA 90095, USA*, [4]*Physics Department, McGill University, Montreal, QC H3A 2T8, Canada*, [5]*Department of Physics, Washington University, St. Louis, MO 63130, USA*, [6]*School of Physics and Astronomy, University of Leeds, Leeds, LS2*

9JT, UK, [7]*Harvard-Smithsonian Center for Astrophysics, 60 Garden Street, Cambridge, MA 02138, USA*, [8]*Argonne National Laboratory, 9700 S. Cass Avenue, Argonne, IL 60439, USA*, [9]*School of Physics, University College Dublin, Belfield, Dublin 4, Ireland*, [10]*School of Physics, National University of Ireland, Galway, Ireland*, [11]*Astronomy Department, Adler Planetarium and Astronomy Museum, Chicago, IL 60605, USA*, [12]*Department of Physics, Purdue University, West Lafayette, IN 47907, USA* , [13]*Department of Physics and Astronomy, Barnard College, Columbia University, NY 10027, USA*, [14]*Santa Cruz Institute for Particle Physics and Department of Physics, University of California, Santa Cruz, CA 95064, USA*, [15]*Laboratoire Leprince-Ringuet, Ecole Polytechnique, CNRS/IN2P3, F-91128 Palaiseau, France*, [16]*Department of Physics and Astronomy, University of Utah, Salt Lake City, UT 84112, USA*, [17]*Enrico Fermi Institute, University of Chicago, Chicago, IL 60637, USA*, [18]*Department of Physics and Astronomy, Iowa State University, Ames, IA 50011, USA*, [19]*Department of Physics and Astronomy, University of Iowa, Van Allen Hall, Iowa City, IA 52242, USA*, [20]*Department of Physics, Pittsburg State University, 1701 South Broadway, Pittsburg, KS 66762, USA*, [21]*Department of Physics, Anderson University, 1100 East 5th Street, Anderson, IN 46012*, [22]*Department of Life and Physical Sciences, Galway-Mayo Institute of Technology, Dublin Road, Galway, Ireland*, [23]*European Southern Observatory, Karl-Schwarzschild-Strasse 2, 85748 Garching, Germany*, [24]*Kavli Institute for Cosmological Physics, University of Chicago, Chicago, IL 60637, USA*, [25]*Department of Applied Physics and Instrumentation, Cork Institute of Technology, Bishopstown, Cork, Ireland*, [26]*National Radio Astronomy Observatory, Socorro, NM 87801, USA*, [27]*Physics Department, 333 Workman Center, New Mexico Institute of Mining and Technology, 801 Leroy Place, Socorro, NM 87801, USA*, [28]*Department of Physics and Astronomy, University of Alabama, Tuscaloosa, AL 35487, USA*, [29]*ISR-2, MS-D436, Los Alamos National Laboratory, Los Alamos, NM 87545, USA*, [30]*Department of Astronomy, University of California, Los Angeles, CA 90095-1547, USA*, [31]*Max-Planck-Institut für Kernphysik, P.O. Box 103980, D-69029 Heidelberg, Germany*, [32]*Yerevan Physics Institute, 2 Alikhanian Brothers St., 375036 Yerevan, Armenia*, [33]*Centre d'Etude Spatiale des Rayonnements, CNRS/UPS, 9 av. du Colonel Roche, BP 4346, F-31029 Toulouse Cedex 4, France*, [34]*Universität Hamburg, Institut für Experimentalphysik, Luruper Chaussee 149, D-22761 Hamburg, Germany*, [35]*Institut für Physik, Humboldt-Universität zu Berlin, Newtonstr. 15, D-12489 Berlin, Germany*, [36]*LUTH, Observatoire de Paris, CNRS, Université Paris Diderot, 5 Place Jules Janssen, 92190 Meudon, France*, [37]*IRFU/DSM/CEA, CE Saclay, F-91191 Gif-sur-Yvette, Cedex, France*, [38]*University of Durham, Department of Physics, South Road, Durham DH1 3LE, U.K.*, [39]*Unit for Space Physics, North-West University, Potchefstroom 2520, South Africa*, [40]*Laboratoire Leprince-Ringuet, Ecole Polytechnique, CNRS/IN2P3, F-91128 Palaiseau, France*, [41]*Laboratoire d'Annecy-le-Vieux de Physique des Particules, CNRS/IN2P3, 9 Chemin de Bellevue - BP 110 F-74941 Annecy-le-Vieux Cedex, France*, [42]*Astroparticule et Cosmologie (APC), CNRS, Universite Paris 7 Denis Diderot, 10, rue Alice Domon et Leonie Duquet, F-75205 Paris Cedex 13, France; UMR 7164 (CNRS, Université Paris VII, CEA, Observatoire de Paris)*, [43]*Dublin Institute for Advanced Studies, 5 Merrion Square, Dublin 2, Ireland*, [44]*Landessternwarte, Universität Heidelberg, Königstuhl, D-69117 Heidelberg, Germany*, [45]*Laboratoire de Physique Théorique et*

Astroparticules, Université Montpellier 2, CNRS/IN2P3, CC 70, Place Eugène Bataillon, F-34095 Montpellier Cedex 5, France, [46]*Universität Erlangen-Nürnberg, Physikalisches Institut, Erwin-Rommel-Str. 1,D-91058 Erlangen, Germany*, [47]*Laboratoire d'Astrophysique de Grenoble, INSU/CNRS, Université Joseph Fourier, BP 53, F-38041 Grenoble Cedex 9, France* , [48]*Institut für Astronomie und Astrophysik, Universität Tübingen, Sand 1, D-72076 Tübingen, Germany*, [49]*LPNHE, Université Pierre et Marie Curie Paris 6, Université Denis Diderot Paris 7, CNRS/IN2P3, 4 Place Jussieu, F-75252, Paris Cedex 5, France*, [50]*Charles University, Faculty of Mathematics and Physics, Institute of Particle and Nuclear Physics, V Holešovičkách 2, 180 00*, [51]*Institut für Theoretische Physik, Lehrstuhl IV: Weltraum und Astrophysik, Ruhr-Universität Bochum, D-44780 Bochum, Germany*, [52]*University of Namibia, Private Bag 13301, Windhoek, Namibia*, [53]*Obserwatorium Astronomiczne, Uniwersytet Jagielloński, ul. Orla 171, 30-244 Kraków, Poland*, [54]*Nicolaus Copernicus Astronomical Center, ul. Bartycka 18, 00-716 Warsaw, Poland*, [55]*School of Physics & Astronomy, University of Leeds, Leeds LS2 9JT, UK*, [56]*School of Chemistry & Physics, University of Adelaide, Adelaide 5005, Australia*, [57]*Toruń Centre for Astronomy, Nicolaus Copernicus University, ul. Gagarina 11, 87-100 Toruń, Poland*, [58]*Instytut Fizyki Jądrowej PAN, ul. Radzikowskiego 152, 31-342 Kraków, Poland*, [59]*European Associated Laboratory for Gamma-Ray Astronomy, jointly supported by CNRS and MPG*, [60]*Supported by CAPES Foundation, Ministry of Education of Brazil*, [61]*ETH Zurich, CH-8093 Switzerland*, [62]*INAF National Institute for Astrophysics, I-00136 Rome, Italy*, [63]*Universidad Complutense, E-28040 Madrid, Spain*, [64]*Technische Universität Dortmund, D-44221 Dortmund, Germany*, [65]*Universitat Autònoma de Barcelona, E-08193 Bellaterra, Spain*, [66]*Università di Padova and INFN, I-35131 Padova, Italy*, [67]*Inst. de Astrofísica de Canarias, E-38200 La Laguna, Tenerife, Spain*, [68]*University of Łódź, PL-90236 Lodz, Poland*, [69]*Deutsches Elektronen-Synchrotron (DESY), D-15738 Zeuthen, Germany*, [70]*Max-Planck-Institut für Physik, D-80805 München, Germany*, [71]*Università di Siena, and INFN Pisa, I-53100 Siena, Italy*, [72]*Universitat de Barcelona (ICC/IEEC), E-08028 Barcelona, Spain*, [73]*Universität Würzburg, D-97074 Würzburg, Germany*, [74]*IFAE, Edifici Cn., Campus UAB, E-08193 Bellaterra, Spain*, [75]*Depto. de Astrofisica, Universidad, E-38206 La Laguna, Tenerife, Spain*, [76]*Università di Udine, and INFN Trieste, I-33100 Udine, Italy*, [77]*Institut de Cienciès de l'Espai (IEEC-CSIC), E-08193 Bellaterra, Spain*, [78]*Inst. de Astrofísica de Andalucia (CSIC), E-18080 Granada, Spain*, [79]*University of California, Davis, CA-95616-8677, USA*, [80]*Tuorla Observatory, Turku University, FI-21500 Piikkiö, Finland*, [81]*Inst. for Nucl. Research and Nucl. Energy, BG-1784 Sofia, Bulgaria*, [82]*INAF/Osservatorio Astronomico and INFN, I-34143 Trieste, Italy*, [83]*ICREA, E-08010 Barcelona, Spain*, [84]*Università di Pisa, and INFN Pisa, I-56126 Pisa, Italy*, [85]*supported by INFN Padova*, [86]*deceased*.